Available online at www.sciencedirect.com
ScienceDirect
Journal of the European Ceramic Society 30 (2010) 199–204
www.elsevier.com/locate/jeurceramsoc

Non-destructive three-dimensional Raman analysis of domain orientation in barium titanate single-crystal

Giuseppe Pezzotti *, Masayuki Higashino, Keisuke Tsuji, Wenliang Zhu

RIN-Research Institute for Nanoscience & Ceramic Physics Laboratory, Kyoto Institute of Technology, Matsugasaki, Sakyo-ku, 606-8585 Kyoto, Japan

Available online 27 May 2009

Abstract

Ferroelectric domain orientation in barium titanate ($BaTiO_3$; BT) single-crystal has been investigated with respect to its geometrical distribution in the solid angle by using polarised Raman spectroscopy. After retrieving the angular dependence of the intensity of selected Raman modes of BT and their defocusing properties at selected laser wavelength (in-depth probe response function), both *in-plane* and *out-of-plane* domain fractions could be visualised and mapped with microscopic resolution by Raman spectroscopic assessments. It is demonstrated that polarised Raman spectroscopy is a valuable and efficient tool for fully 3D, non-destructive assessments of domain orientation in ferroelectrics.

Keywords: B. Non-destructive evaluation; B. Spectroscopy; D. $BaTiO_3$ and titanates

1. Introduction

In the continuous search for advanced performances and miniaturization of ceramic capacitors, materials and structural elements with high dielectric permittivity and high reliability on the sub-micron scale are the object of intensive research. Tailoring smaller interlayer thicknesses with higher capacitance motivates a common trend towards miniaturization. This is particularly true for multilayer capacitors, but the same concept can be extended to thin-film technology, which nowadays has gained much attention for application in solid-state memories and other miniaturized devices.[1] Single-crystalline single-domain BT has been deeply studied because of its highly anisotropic permittivity, whose value greatly exceeds that recorded in polycrystalline samples with the same nominal composition. The higher permittivity values are ascribed to small oscillations of domain walls, a phenomenon which, on the other hand, is also mainly responsible for the dissipation factor. Residual stresses, which are in turn influenced by the developed domain texture, also influence the electrical properties. The stress effect is particularly critical in thin films and at the interfaces with the electrodes. Therefore, the development of an analytical method capable to reliably and easily reveal domain texture in ferroelectric ceramics is urgently required, as it should greatly assists a deterministic control of dielectric properties.[2] In addition, the establishment of a fully non-destructive evaluation technique capable of investigating the dielectric device locally and in elements buried below the surface could greatly contribute to the advancement of production processes and to the enhancement of product reliability.

Domain sampling and orientation analyses in ferroelectrics have been so far performed by X-ray diffraction[3] and microdiffraction,[4] neutron diffraction,[5] scanning force microscopy,[6] and Raman spectroscopy,[7–11] which has been also applied to residual stress assessments in BT-based Ni-MLCC.[12] In two previous works[10,11] we have developed a Raman tensorial formalism based on two Euler angles in space, which allows determining domain fractions of *c*-axis oriented domains in a fully three-dimensional (3D) fashion. Raman spectroscopy appears particularly advantageous over other analytical techniques for BT texture analysis, as it combines high spatial resolution and flexibility in quickly scanning relatively large areas of the sample with a compact equipment. The use of this technique, coupled with the physical understanding of the character of the probe, provides an invaluable tool for in-depth analyses, which perfectly matches the industrial needs in terms of non-destructive, contactless and highly spatially resolved measurements.

In this paper, polarised Raman spectroscopy has been applied to analyse domain textures in a bulk BT single-crystal. The angular dependences of selected Raman modes intensity and

* Corresponding author. Tel.: +81 075 724 7568; fax: +81 075 724 7568.
E-mail address: pezzotti@chem.kit.ac.jp (G. Pezzotti).

0955-2219/$ – see front matter © 2009 Elsevier Ltd. All rights reserved.
doi:10.1016/j.jeurceramsoc.2009.04.016

wavenumber have been first investigated, and defocusing experiments have been carried out in order to precisely calibrate the dimensions of the Raman probe when focused inside the semi-transparent BT body. A deconvolution procedure has been then established in order to perform in-depth mapping of BT domains, and it has been subsequently applied to a BT single-crystal after being subjected to compressive uniaxial loading. The domain texture developed upon loading inside the crystal has finally been displayed in 3D fashion, proving the advantages of the Raman approach to non-destructive evaluations of ferroelectric ceramics.

2. Experimental

A BT single-crystal specimen (*a*-plane) with dimensions 10 mm × 10 mm × 10 mm, supplied by Murata Manufacturing Co., Ltd. (Nagaokakyo, Kyoto, Japan), was used in this study. The identification of *a*-plane was preliminary made according to X-ray diffraction and it refers to the crystallographic axis of the tetragonal crystal group. The investigated surface of the BT crystal was finely polished by diamond paste prior to Raman characterization.

Polarised Raman spectroscopic experiments were carried out in a backscattering configuration with a triple monochromator (T-64000, Horiba/Jobin-Yvon, Kyoto, Japan) equipped with liquid nitrogen-cooled Charge Coupled Device (CCD). Excitation was provided by the 488 nm line of a Ar-ion laser (Stabilite 2017, Spectra-Physics, Mountain View, CA), with a maximum power of 40 mW. The reference system was chosen in order to assign the *x*, *y*, *z* Cartesian axes (*i.e.*, the laboratory reference) to *a*, *b* = *a*, *c*, axes of a tetragonal crystallographic structure, respectively. Spectra were acquired in parallel $x(yy)\bar{x}$ configuration with a 100× (NA = 0.9) objective lens, which allowed us to reduce the diameter of the laser beam waist to less than 1 μm on the material surface. A half-wave plate was employed to compensate for the polarisation dependence of the monochromator. Experiments were conducted in a confocal probe configuration, with the pinhole aperture of the optical circuit set to 100 μm.[13]

Spectral positions and intensities of BT Raman spectra were measured upon rotating the single-crystalline sample under polarised light. A rotating jig has been used and care was made in fixing the measurement location during rotation by carefully aligning the jig centre with the objective focal axis. A full rotation of the sample was performed and Raman spectra were measured (with 10° steps) rotating the angle θ between the *c*-axis of the BT single-crystal and the *y*-axis of the laboratory reference system (laser polarisation direction). Prior to Raman characterization, the sample was subjected to uniaxial compression along its *c*-axis, in order to generate an internal domain pattern. The applied load was below the critical threshold for fracture, but it sufficed to introduce domain patterns along internal shear bands. Domain orientation analysis has been then performed in-depth along the *a*-axis; maps have been collected at in-depth intervals between 40 and 60 μm inside the sample.

Spectral lines were analysed with the aid of a commercial software package (Labspec 4.02, Horiba/Jobin-Yvon, Tokyo, Japan). Fitting was performed with Gaussian–Lorentzian spectral modes after subtracting a baseline; first trial spectra were drawn according to the vibrational modes described in the available literature.[14] Defocusing experiments were deconvoluted along the in-depth direction in order to retrieve domain fraction maps in different planes below the sample surface. The mathematical procedure needed to obtain deconvoluted maps has been carried out with the aid of computational software (Mathematica 5.2; Wolfram Research Inc., Champaign, IL).

3. Theoretical background

3.1. Domain fractions from Raman scattering in ferroelectrics

The relative intensity of Raman bands strongly depends on crystal orientation and on the polarisation geometry of the adopted optical configuration. Such dependence can be expressed as[15]:

$$I \propto |e_i \Re e_s|^2, \tag{1}$$

where I is the reflected Raman intensity, e_i and e_s are the unit polarisation vectors of the electric field of the incident and scattered laser beam, respectively, while $\Re$ represents the Raman scattering tensor of the particular vibrational mode under consideration. The Raman tensor is a second rank tensor and, for the A_g, B_1 and E_g vibrational modes of a tetragonal crystal belonging to the C_{4v} space group, it takes the forms given in (2):

$$\Re_{A_g} = \begin{bmatrix} a & 0 & 0 \\ 0 & a & 0 \\ 0 & 0 & b \end{bmatrix}, \ \Re_{B_1} = \begin{bmatrix} c & 0 & 0 \\ 0 & -c & 0 \\ 0 & 0 & 0 \end{bmatrix}, \ \Re_{E_y} = \begin{bmatrix} 0 & 0 & 0 \\ 0 & 0 & e \\ 0 & e & 0 \end{bmatrix}. \tag{2}$$

The components of the above Raman tensors represent the scattering components along various directions of the tetragonal crystal. When a rotation, which involves components with respect to both *y*-axis and *z*-axis, describes the inclination of the *c*-axis with respect to sample surface propagation direction of the laser, the *in-plane* polarisation direction of the laser can be described according to an orthogonal transformation matrix, Φ_{xyz} (and its inverse, $\tilde{\Phi}_{xyz}$), as follows:

$$\Re_{j,xyz} = \Phi_{xyz} \Re_j \tilde{\Phi}_{xyz}, \tag{3}$$

with the transformation matrix is given as:

$$\Phi_{xyz} = \begin{pmatrix} -\cos\theta \sin\psi & \cos\psi & \sin\theta \sin\psi \\ -\cos\theta \cos\psi & -\sin\psi & \sin\theta \cos\psi \\ \sin\theta & 0 & \cos\theta \end{pmatrix}, \tag{4}$$

where θ is the *in-plane* angle (*i.e.*, a solid rotation of the *c*-axis with respect to the *y*-axis), and ψ is the *out-of-plane* angle

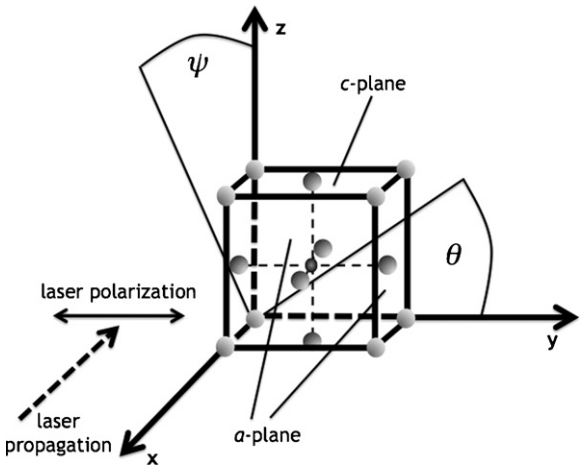

Fig. 1. Schematic showing the Cartesian axes, the crystal structure/orientation with respect to loading direction, Euler angles and polarisation directions adopted in this study.

(*i.e.*, a solid rotation of the *c*-axis with respect to the *z*-axis). An explanatory draft showing the relationship between the tetragonal BT crystal axes, the probe polarisation axis, the rotation angles, and the axis of uniaxial compressive loading is given in Fig. 1. Eqs. (1) and (2) can then be modified according to (3) and (4), to obtain:

$$I^{||}_{A_g} \propto |a\ \cos^2\ \theta + \sin^2\ \theta(a\ \cos^2\ \psi + b\ \sin^2\ \psi)|^2, \tag{5}$$

$$I^{||}_{B_1} \propto |c(\cos^2\ \theta\ \cos\ 2\psi + \sin^2\ \theta\ \cos^2\ \psi)|^2, \tag{6}$$

$$I^{||}_{E_g} \propto |e\ \sin\ \theta\ \sin\ 2\psi|^2, \tag{7}$$

where the superscript || refers to the parallel $x(yy)\bar{x}$ polarised configuration, adopted throughout this work. Once the Raman tensor of the investigated material has been determined by monitoring the intensity variation upon rotation of the crystal under a fixed configuration of polarised light,[10] the relative intensities of two selected modes (with respect to the same reference mode, *i.e.*, A_g/B_1 and E_g/B_1) can be used to determine both *in-plane* and *out-of-plane* angles at each investigated location.[11] From a close look to Eq. (7), it is clear that the intensity of the E_g mode in parallel configuration of the scattered light is suppressed at angular selections corresponding to $\psi = \pi/2$. In other words, the *out-of-plane* orientation of domains can be directly estimated from the relative intensity of the $E(LO_4)$ band in parallel configuration. The equations that locate the *out-of-plane* orientation angle of the crystal *c*-axis and the volume fraction, δ_{OP}, of *c*-axis oriented domains in such a plane can be then given, as follows[11]:

$$\frac{I^{||}_{E_g}}{I^{||}_{B_1}} = \Lambda\frac{|e\ \sin\ \theta\ \sin\ 2\psi|^2}{|c\ \cos^2\ \theta\ \cos\ 2\psi + \sin^2\ \theta\ \cos^2\ \psi|^2} + \gamma, \tag{8}$$

$$\delta_{OP} = \frac{I^{||}_{E_g}/I^{||}_{B_1}}{(I^{||}_{E_g}/I^{||}_{B_1})_{\max}}, \tag{9}$$

where Λ and γ are instrumental constants, which should be obtained experimentally according to the Raman device employed. In addition, the *in-plane* orientation angle of the crystal *c*-axis and the fraction, δ_{IP}, of *c*-axis oriented domains in such a plane, is as follows[10]:

$$\frac{I^{||}_{A_g}}{I^{||}_{B_1}} = \Lambda\frac{|a\ \cos^2\ \theta + b\ \sin^2\ \theta|^2}{|c\ \cos^2\ \theta|^2} + \gamma, \tag{9}$$

$$\delta_{IP} = \frac{b^2}{(I^{||}_{A_g}/I^{||}_{B_1})c^2 - (a^2 - b^2)}, \tag{10}$$

Eqs. (10) and (8) can therefore be suitably used to calculate the *in-plane* and *out-of-plane* fractions of *c*-axis oriented domains, respectively.

3.2. Determination of in-depth and lateral probe response function

In Raman spectroscopy, the laser beam is assumed to have a Gaussian distribution of intensity in the *x*, *y* plane around the geometric–optical focus, and a Lorentzian distribution along the *z*-axis.[13,16] When a laser beam is focused at a given point (x_0, y_0, z_0), the observed spectrum generates from all the illuminated points within a region centred at (x_0, y_0, z_0):

$$I_{obs} \propto \int_{-\infty}^{+\infty}\int_{-\infty}^{+\infty}\int_{0}^{+\infty} e^{-2\alpha z} \times \frac{p^2}{p^2 + (z - z_0)^2} e^{\left[-2\frac{(x-x_0)^2+(y-y_0)^2}{w^2}\right]} dxdydz, \tag{11}$$

where α is the absorption coefficient of the material under investigation, *p* the probe response parameter in the *z*-direction, *w* the probe response parameter in the *x*-, *y*-directions (half the beam width). Eq. (11) contains a three-dimensional integral, which theoretically cannot be separated into independent parts, but could be simplified in some particular conditions. For example, when the intensity variation (or the property information conveyed in the spectrum) within the probe is not pronounced in the *x*-, *y*-directions, the influence of the probe in the *x*, *y* plane can be withdrawn from the integral, which thus reduces to:

$$I_{obs} \propto \int_{0}^{+\infty} e^{-2\alpha z}\frac{p^2}{p^2 + (z - z_0)^2} dz. \tag{12}$$

This is the case of a defocusing scan along the *z*-axis performed at a fixed position in (*x*, *y*), which is the experiment commonly pursued for the determination of the in-depth probe response parameter, *p*.[17] On the other hand, a scanning along the *x*-direction while maintaining the laser focused on the material surface leads to the following modification of Eq. (11):

$$I_{obs} \propto \int_{-\infty}^{+\infty} e^{\left[-2\frac{(x-x_0)^2}{w^2}\right]} dx, \tag{13}$$

which applies for the determination of *w* by displacing in plane the laser probe along, for example, a given *x*-axis across a sharp and straight interface, perpendicular to the sample surface. The body of information described above can be used to determine the effective in-depth probe size, Z_p, which is defined as the

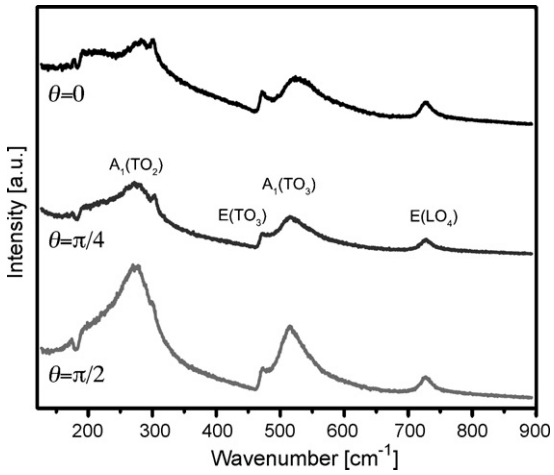

Fig. 2. Parallel $(x(yy)\bar{x})$ polarised Raman spectra of the investigated single-crystalline BT sample for three different orientations of the crystal main axis with respect to the laser light polarisation vector: $\theta = 0$, $\pi/4$, $\pi/2$.

penetration depth that contributes to the 90% of the scattered intensity information:

$$0.9 = \frac{\int_0^{Z_p} e^{-2\alpha z}(p^2/(p^2+z^2))dz}{\int_0^{\infty} e^{-2\alpha z}(p^2/(p^2+z^2))dz}. \quad (14)$$

This parameter, together with the focused beam waist, is sufficient to describe the defocusing properties of the investigated material, and provides a useful tool for subsurface analyses.

4. Results and discussion

Polarised Raman spectra of BT single-crystals are shown in Fig. 2 for $\theta = 0$, $\pi/4$, $\pi/2$, and the modes assigned for the spectra obtained as given in Table 1. As could clearly be seen, A_g modes are greatly enhanced when the *c*-axis of the tetragonal structure is perpendicular to the laser polarisation vector ($\theta = \pi/2$), while on the other hand at $\theta = 0$ they undergo an abrupt intensity decrease. Upon giving a first glance to the collected spectra, the ubiquitous presence of the E_g modes (*cfr.* $E(TO_3)$ and $E(LO_4)$) allows us to conclude that, although the investigated sample is an *a*-plane single-crystal, the compression exerted on it produced a fraction of *out-of-plane c*-oriented domains. In other words, the *c*-axis orientation is no longer perpendicular to the investigated surface, and the material presents mixed *a*-plane and *c*-plane characteristics.

Table 1
Raman mode position for the investigated BT.

Mode	Band position (cm^{-1})
$E(TO_1)$, $E(LO_1)$	180
$A_1(TO_1)$	200
$A_1(TO_2)$	270
$B_1(TO)$, $E(TO_2+LO_2)$	305
$E(LO_3)$	463
$E(TO_3)$	490
$A_1(TO_3)$	515
$E(LO_4)$	715
$A_1(LO_1)$	720

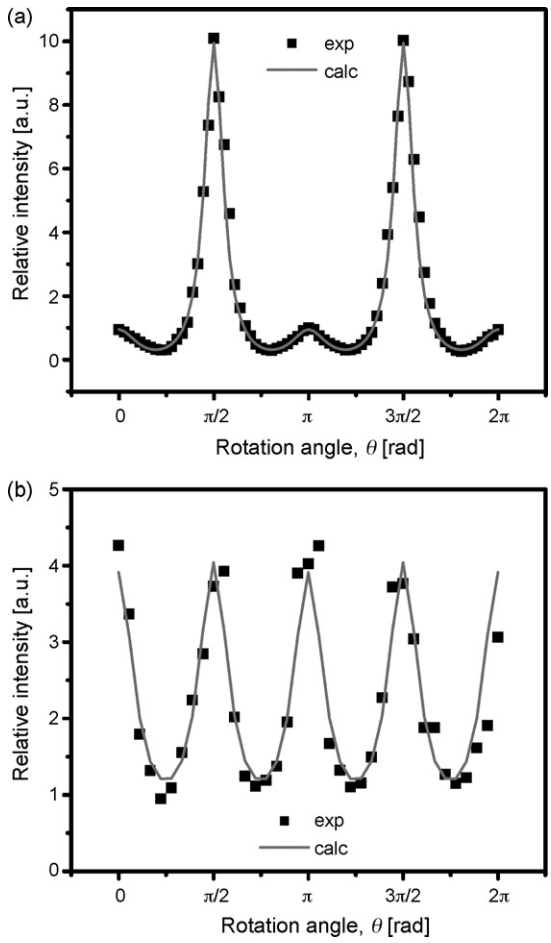

Fig. 3. Angular dependence of (a) $A_1(TO_2)/B_1 + E$ and (b) $E(LO_4)/B_1 + E$ relative intensity upon rotation of the BT single-crystal under a fixed configuration of the polarised light. Solid lines represent theoretical fitting equations.

In this work, the domain orientation has been analysed by monitoring the relative intensity of $A_1(TO_2)$ and $B_1 + E$ modes (*cf.* Table 1) for *in-plane* measurements, and the relative intensity of $E(LO_4)$ and $B_1 + E$ modes for *out-of-plane* measurements. Fig. 3 reports in (a) and (b) the variation upon rotation under fixed polarised light of the relative intensity of $A_1(TO_2)/B_1 + E$ and $E(LO_4)/B_1 + E$ modes, respectively. Solid lines represent fitting by combinations of Eqs. (5)–(7), derived for the *in-plane* case. The different characters of the intensity variation is given by a correspondence between Raman tensor parameters and lattice constants of the tetragonal cell. In Fig. 3(a) the A_g character dominates, and this is related to the *a*-plane of the tetragonal structure. In this case, *a* and *c* lattice constants are involved, and the periodicity is π. On the other hand, in Fig. 3(b), the E_g character, belonging to the *c*-plane of the tetragonal structure, dominates. Being the sole *a* lattice parameter involved, the periodicity is shown as $\pi/2$.

To each value of relative intensity acquired in the focused point an angle can be assigned, whose value is averaged over all the orientations the probe encounters (*i.e.*, the volume of material that contributes to the integrated intensity signal), and the result may therefore be different from the physical reality.

In ferroelectric tetragonal single-crystals, domains may only switch by 90° or 180° from their original position, thus only $\theta = 0$ or $\theta = \pi/2$ orientations are expected. Any other intermediate orientation between these two values has to be ascribed to probe averaging effects, and thus needs to be corrected according to the deconvolution procedure proposed hereafter.

Defocusing experiments have been performed on BT single-crystal in order to obtain preliminary information of probe geometry and dimensions. Raman intensity assessments for both z-axis defocusing (Fig. 4(a)) and x-axis displacements (Fig. 4(b)) have been carried out; in the latter case, the probe has been translated from the outside towards the inside across a sharp edge of the BT sample. In the case of defocus along the z-axis (Fig. 4(a)), data have been corrected for the effect of the refractive index inside the material. Data regression has been performed according to Eqs. (12) and (13) in the case of z-axis and x-axis calibrations, respectively; this led to the determination of the respective probe response parameters, $p = 7.7$ and $w = 3.0\ \mu m$. As can be seen from Fig. 4(b), in the case of defocusing in air in the x-direction, some fitting error is involved; these secondary effects can be ascribed to the sample edge being not sufficiently sharp to mark an abrupt transition while the probe enters the material. From the experiments shown in Fig. 4, the BT probe size has been calculated as $Z_p = 37.7\ \mu m$, while the beam waist (x, y plane) was $2w = 6\ \mu m$.

In this work, in-depth intensity maps have been performed with shifting the probe inside the material (along the z-direction) and with collecting data on a fixed area in the (x, y) planes. Displacement steps between adjacent points were 2 μm on the x-, y-directions and 5 μm in-depth. Since sharp edge appeared for *in-plane* features in the collected maps, the influence of the probe could be neglected on the x, y plane, but the probe-convolution effect was taken into consideration along the z-axis. This is easy to understand if one, for example, considers that a spectrum taken 5 μm below the material surface will convey information not only from the focal plane, but also from points as deep as 40 μm below the focal plane. This consideration clarifies that the retrieved Raman information should be mandatorily deconvoluted along the z-axis in order to correctly assign to each location the proper value of the investigated property.

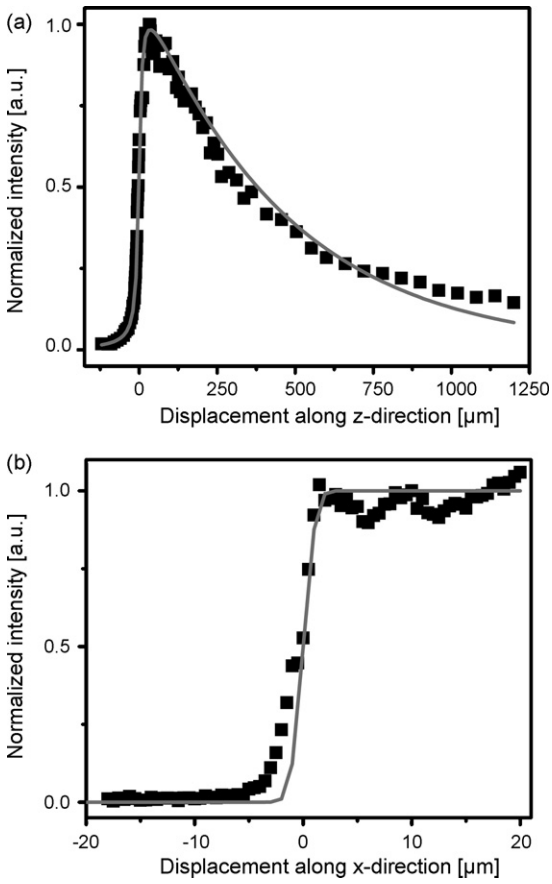

Fig. 4. Intensity variation of BT spectrum upon: (a) in-depth defocusing along the z-axis and (b) horizontal scanning along x-axis across a sharp edge of the sample. Solid lines represent fitting according to Eqs. (12) and (13), respectively.

In this study, we performed the in-depth deconvolution assuming a polynomial model distribution for representing the relative intensity gradients along the z-direction. In-depth relative intensity maps have subsequently been corrected according

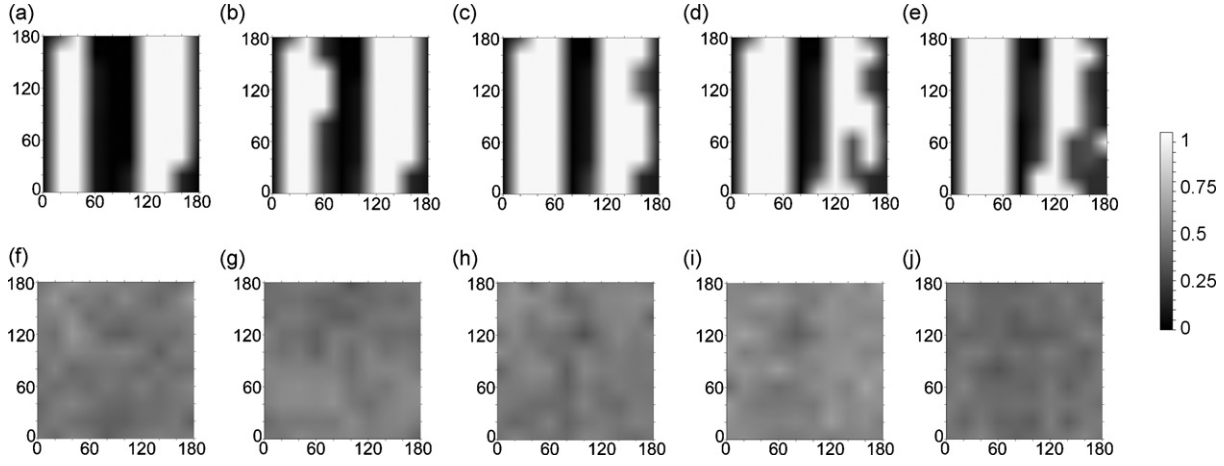

Fig. 5. (a)–(e) *In-plane* fraction of c-axis domain with respect to the laser polarisation direction at depths of 40, 45, 50, 55, 60 μm, respectively. (f)–(j) *Out-of-plane* fraction of c-axis oriented domains with respect to the sample surface, on the same areas of (a)–(e). All metric scales are in μm.

to the following equation, which represents the convoluted relative intensity at the focal point:

$$RI_{obs}(z) = \frac{\int_0^t \{a + bz + cz^2 + dz^3 + ez^4\} \frac{p^2}{p^2+(z-z_f)^2} e^{-2\alpha z} dz}{\int_0^t \frac{p^2}{p^2+(z-z_f)^2} e^{-2\alpha z} dz}, \quad (15)$$

where $RI_{obs}(z)$ is the experimentally retrieved relative intensity value, t is the maximum achievable probe penetration depth for the focused point considered, and z_f is the depth of the focal point. The deconvoluted relative intensity profile was found by adjusting the polynomial model parameters in order to match the retrieved intensity with an iterative procedure. From the deconvoluted Raman intensity values computed at each point of the map, the correspondent domain fractions could be calculated, according to Eqs. (8)–(10).

Results of in-depth domain fraction analysis (after deconvolution) are shown in Fig. 5. The upper part of the figure (Fig. 5(a)–(e)) reports *in-plane* domain fraction at the depth of 40, 45, 50, 55, 60 μm from the surface of the material, while the lower part (Fig. 5(f)–(j)) reports *out-of-plane* domain fractions from the same areas. *In-plane* maps have been calculated assuming $\psi = \pi/2$ (*a*-plane) and considering the influence of E_g modes inside the B_1 mode negligible. Regarding the *in-plane* maps, domains are oriented either at $\theta = 0$ or $\theta = \pi/2$, which demonstrates that the compressive stress produced 90° switching in the single-crystalline body, with a significant twinning of domains. No intermediate orientations were found, and this is regarded as a proof of the effectiveness of the algorithm selected for the deconvolution procedure. On the same areas, *out-of-plane* domain fraction analysis reveals that a slight misalignment of the crystal along the *z*-axis occurred (about 25%), which caused the appearance of *c*-plane features in the Raman spectra of the investigated *a*-plane sample. The overall orientation of the *c*-axis with respect to the sample surface could be estimated as $\psi = 42.5°$.

5. Conclusion

A clear correlation between the relative intensity of Raman bands in a selected polarisation geometry and domain orientation with respect to the polarisation direction of the incident laser was observed in single-crystalline BT. Such a correlation could be consistently rationalised according to a Raman tensorial formalism. As an application of the technique, in-depth domain fraction maps have been collected non-destructively by taking into account the influence of the probe dimensions and upon gradually defocusing the laser probe inside the crystal. A computational procedure, based on the experimental probe response function, has also been proposed for minimizing probe convolutive effects on the detected Raman relative intensity. This study demonstrates that polarised microprobe Raman spectroscopy is a highly advantageous technique for in-depth non-destructive domain orientation analyses in ferroelectric materials.

Acknowledgment

The authors would like to kindly acknowledge Mr. Yasuhisa Yamashita (former Murata Manufacturing Co., Ltd.) for supplying the single-crystalline BT specimen.

References

[1]. Shaw, T. M., Suo, Z., Huang, M., Liniger, E., Laibowitz, R. B. and Baniecki, J. D., The effect of stress on the dielectric properties of barium strontium titanate thin films. *Appl. Phys. Lett.*, 1999, **75**, 2129–2131.
[2]. Moulson, A. J. and Herbert, J. M., *Electroceramics*. Wiley, Southern Gate, 2003, p. 312.
[3]. Subbarao, E. C., McQuarrie, M. C. and Buessem, W. R., Domain effects in polycrystalline barium titanate. *J. Appl. Phys.*, 1957, **28**, 1194–1200.
[4]. Tamura, N., MacDowell, A. A., Celestre, R. S., Padmore, H. A., Valek, B., Bravman, J. C. *et al.*, High spatial resolution grain orientation and strain mapping in thin films using polychromatic submicron X-ray diffraction. *Appl. Phys. Lett.*, 2002, **80**, 3724–3726.
[5]. Forrester, J. S., Kisi, E. H. and Studer, A. J., Direct observation of ferroelastic domain switching in polycrystalline $BaTiO_3$ using in situ neutron diffraction. *J. Eur. Ceram. Soc.*, 2005, **25**, 447–454.
[6]. Munoz-Saldana, J., Schneider, G. A. and Eng, L. M., Stress induced movement of ferroelastic domain walls in $BaTiO_3$ single crystals evaluated by scanning force microscopy. *Surf. Sci.*, 2001, **480**, 402–410.
[7]. Li, Z., Foster, C. M., Dai, X.-H., Xu, X.-Z., Chan, S.-K. and Lam, D. J., Piezoelectrically-induced switching of 90° domains in tetragonal $BaTiO_3$ and $PbTiO_3$ investigated by micro-Raman spectroscopy. *J. Appl. Phys.*, 1992, **71**, 4481–4486.
[8]. Pojprapai(Imlao), S., Jones, J. L. and Hoffman, M., Determination of domain orientation in lead zirconate titanate ceramics by Raman spectroscopy. *Appl. Phys. Lett.*, 2006, **88**, 1629031–1629033.
[9]. Deluca, M., Sakashita, T. and Pezzotti, G., Polarized Raman scattering of domain structures in polycrystalline lead zirconate titanate. *Appl. Phys. Lett.*, 2007, **90**, 0519191–519193.
[10]. Deluca, M., Higashino, M. and Pezzotti, G., Raman tensor elements for tetragonal $BaTiO_3$ and their use for in-plane domain texture assessments. *Appl. Phys. Lett.*, 2007, **91**, 0919061–919063.
[11]. Pezzotti, G., Matsutani, A., and Zhu, W., Spectroscopic assessments of domain texture in barium titanate: I, Confocal Raman polarization analysis. *J. Am. Ceram. Soc.*, submitted for publication.
[12]. Sakashita, T., Nakamura, K., Pezzotti, G. and Chazono, H., Raman piezospectroscopic investigation of microscopic residual stresses in Ni-MLCC devices. *Key Eng. Mater.*, 2006, **301**, 31–36.
[13]. Zhu, W. and Pezzotti, G., Spatially resolved stress analysis in Al_2O_3/3Y-TZP multilayered composite using confocal fluorescence spectroscopy. *Appl. Spectrosc.*, 2005, **59**, 1042–1048.
[14]. El Marssi, M., Le Marrec, F., Lukyanchuk, I. A. and Karkut, M. G., Ferroelectric transition in an epitaxial barium titanate thin film: Raman spectroscopy and X-ray diffraction study. *J. Appl. Phys.*, 2003, **94**, 3307–3312.
[15]. Loudon, R., The Raman effect in crystals. *Adv. Phys.*, 1964, **13**, 423–482.
[16]. Born, M. and Wolf, E., *Principles of Optics*. Pergamon Press, Oxford, 1985, p. 441.
[17]. Lipkin, D. M. and Clarke, D. R., Sample-probe interactions in spectroscopy: sampling microscopic property gradients. *J. Appl. Phys.*, 1995, **77**, 1855–1863.